ChemSystemsChem

Chemistry Europe
European Chemical Societies Publishing

Accepted Article

Title: Complex coacervation and compartmentalized conversion of prebiotically relevant metabolites

Authors: Iris B. A. Smokers, Merlijn H. I. van Haren, Tiemei Lu, and Evan Spruijt

To be cited as: *ChemSystemsChem* **2022**, e202200004

Link to VoR: https://doi.org/10.1002/syst.202200004

WILEY-VCH

Complex coacervation and compartmentalized conversion of prebiotically relevant metabolites

Iris B. A. Smokers[‡[a]], Merlijn H. I. van Haren[‡[a]], Tiemei Lu[[a]] and Dr. Evan Spruijt*[[a]]

[a] *Institute for Molecules and Materials, Radboud University, Heyendaalseweg 135, 6523 AJ Nijmegen, The Netherlands*

[‡] These authors contributed equally. * Correspondence: e.spruijt@science.ru.nl

Keywords: protocells, complex coacervation, compartmentalization, prebiotic chemistry

Abstract

Metabolism and compartmentalization are two of life's most central elements. Constructing synthetic assemblies based on prebiotically relevant molecules that combine these elements can provide insight into the requirements for the formation of life-like protocells from abiotic building blocks. In this work, we show that a wide variety of small anionic metabolites can form complex coacervate protocells with oligoarginine (R_{10}) by phase separation. The coacervate stability can be rationalized by the molecular structure of the metabolites, and we show that three negative charges for carboxylates, or two negative charges complemented with an unsaturated moiety for phosphates and sulfates is sufficient for phase separation. The metabolites remain reactive after compartmentalization, and we show that protometabolic reactions can induce coacervate formation. The resulting coacervates can localize other metabolites and enhance their conversion. Finally, reactions of compartmentalized metabolites can also alter the physicochemical properties of the coacervates and ultimately lead to protocell dissolution. These results reveal the intricate interplay between (proto)metabolic reactions and coacervate compartments, and show that coacervates are excellent candidates for metabolically active protocells.

10.1002/syst.202200004

Graphical abstract

Metabolically active coacervates combine two important hallmarks of life: metabolism and compartmentalization. Here we show that a wide range of prebiotic metabolites can form complex coacervate protocells with oligoarginine. Prebiotically plausible conversions of the metabolites can give rise to active coacervate formation, are enhanced inside the coacervate microenvironment and can, in turn, affect the stability of the coacervate compartment.

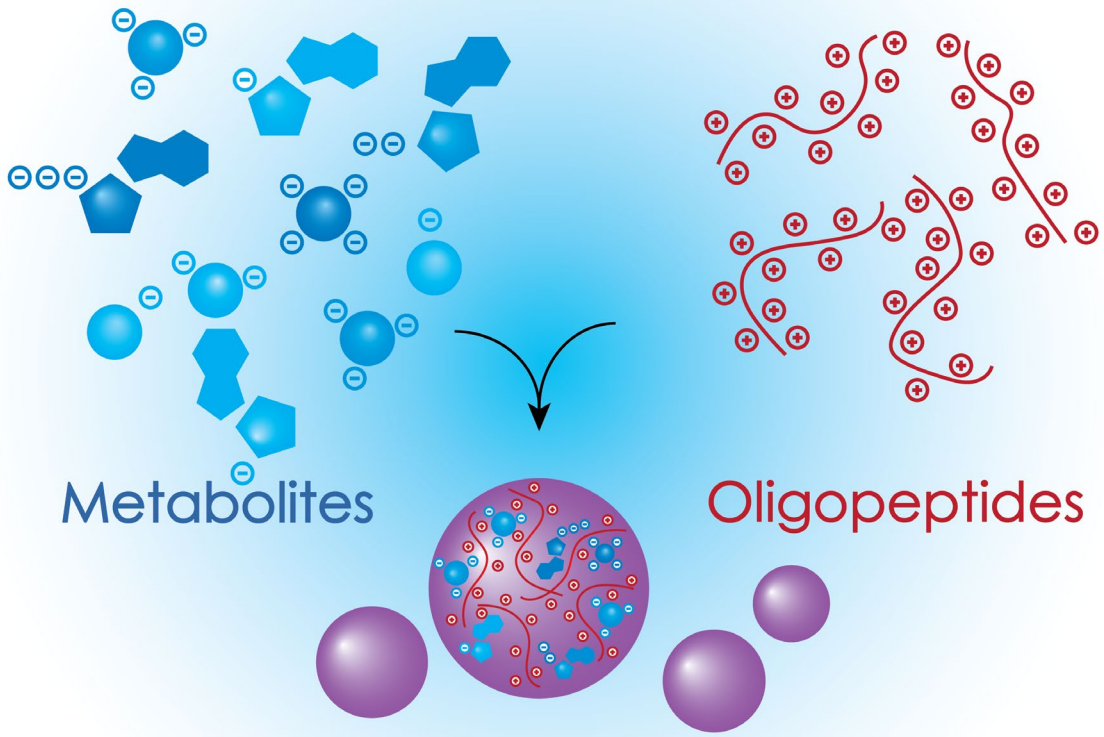

Introduction

Metabolism and compartmentalization are fundamental elements of life.[1-2] Prebiotic routes to form and convert central metabolites and ways to compartmentalize them are therefore of utmost relevance. Prebiotic reactions of common metabolites such as ATP, NADH and citric acid have been studied extensively, as these molecules play a key role across the tree of life in reaction pathways such as the tricarboxylic acid (TCA) cycle, which releases energy to fuel various cellular processes.[3-9] However, their concentrations on the early Earth were likely very low, slowing down these protometabolic reactions to non-viable pace. Moreover, some of the developed reactions proceed under mutually incompatible conditions of, for instance, pH, redox potential or light. Compartmentalization of reagents can increase local concentrations and create distinct chemical microenvironments, and might have therefore been an important step in gaining sufficiently high reaction rates and selectivity at the origins of life.[10-13]

Compartmentalization through self-assembly of amphiphiles into vesicles has long been considered as the general mechanism for the formation of the first protocells.[14] However, this encapsulation was likely inefficient without the presence of active exchange of components by complex transport machineries, limiting the local concentrations that could be reached inside these protocells.[15] Since the discovery that membraneless organelles in modern cells can form by liquid-liquid phase separation (LLPS), the analogous formation of protocells by LLPS has received increasing interest.[16-18] Multiple weak associative interactions, such as charge-charge and cation-π interactions, between molecules can drive LLPS to form (complex) coacervates, which are droplets of a solute-rich phase dispersed in a dilute continuous phase.[19-20] If the associative interactions occur between different parts of the same molecule, the resulting coacervates are formed by a single solute species, and are called simple coacervates.[18-19] If the associative interactions occur between two or more molecules, which are, for example, oppositely charged, coacervates are formed by at least two solute species, and are called complex coacervates. Both simple and complex coacervates have been shown to spontaneously concentrate reagents and increase reaction rates,[21-23] and recently it has been shown that they can even be formed by prebiotically relevant mononucleotides and short homopeptides containing just five residues.[11, 24] Moreover, droplets made from peptides with prebiotically relevant low molecular weight

were found to be more effective at generating distinct pH microenvironments, accumulating RNA and stabilizing its secondary structure, than coacervates formed by high molecular weight polyelectrolytes.[24]

Since many key metabolites have multiple negative charges, we hypothesized that these metabolites could similarly undergo complex coacervation to become compartmentalized inside protocells, and that these protocells could be capable of sustaining metabolic reactions. While the large majority of complex coacervates in literature are composed of long polymers, a few examples of complex coacervates made of small metabolites[11, 24-26] and other low molecular weight compounds[22-23] have been reported. AMP and citric acid have been shown to phase separate with oligoarginine and protamine, a 4.2 kDa protein containing 21 arginine residues, respectively.[24-25] Additionally, pyrophosphate and triphosphate were found to phase separate with lysozyme and histatin-5, both of which have a net charge of z = +6 or +7 at the investigated pH.[26-27] However, a systematic analysis of phase separation of prebiotic metabolites is still lacking, and the metabolic activity of the coacervate protocells is unexplored.

Here, we show that anionic metabolites with at least three charges, or two when complemented with additional cation-π or π-π interaction sites, are able to form complex coacervates with the short peptide oligoarginine (R_{10}). We compare various types of prebiotically relevant metabolites, including carboxylic acids, phosphates and sulfates in their ability to form coacervates, and show that their stability varies significantly due to small differences in molecular structures, such as their degree of unsaturation, hydrogen bonding ability and charge density. We show that these metabolites continue to undergo metabolic reactions and that these reactions can control compartmentalization and vice versa: metabolite conversion can give rise to active formation and growth of coacervate protocells, metabolite conversion can be accelerated inside coacervate compartments, and finally, metabolite conversion inside coacervates can alter the nature of the protocells, by creating products that affect the stability of the coacervates. These observations reveal the intricate interplay between protometabolic reactions and coacervate compartments, and show that coacervates are excellent candidates to compartmentalize protometabolic networks.

Results and discussion

Metabolites with at least two negative charges form stable coacervates with oligoarginine

Inspired by the central importance of metabolism in living systems, we wondered if key prebiotic metabolites could be compartmentalized by liquid-liquid phase separation, and if so, how propensity for phase separation is linked to the molecular structure. To answer these questions, we investigated three classes of metabolites and related small molecules: carboxylic acids, phosphates, and sulfite/sulfates (structures shown in Figure 1 and Table S1). We selected di- and tricarboxylic acids from the tricarboxylic acid (TCA) and 4-hydroxy-2-ketoglutarate (HKG)[4] cycles, complemented with an aromatic tricarboxylic acid. Phosphates were selected that are part of the cellular respiration, like ATP, which functions as biochemical energy currency, or prebiotic analogues, such as triphosphate and trimetaphosphate (TMP). Finally, we selected sulfites and sulfates and some iron complexes, because of their possible relevance in protometabolic reactions on early Earth.[28-29] For each molecule, we determined its ability to phase separate with a short oligoarginine peptide (R_{10}). Oligoarginine was chosen as the model cation because it is known to form coacervates with small molecules like AMP and because arginine-containing peptides have been suggested to occur on the early Earth.[24, 30] To keep the system as simple as possible, stock solutions were adjusted to a pH of 7.0 ± 0.3 with HCl and NaOH and no buffer was used, since excess ions present in the buffer can screen the electrostatic interactions and mask a potential phase separation. We decided to compare the ability of metabolites to form coacervates at equal concentration, so the concentration of all metabolites is fixed at 5 mM and R_{10} at 5 mM of arginine residues.

We found that carboxylic acid metabolites with three charges (z = -3) were all able to form coacervate droplets with R_{10}, while monocarboxylic acids (MCA) and dicarboxylic acid (DCA) resulted in homogenous solutions, as determined by optical microscopy and turbidity measurements (Table S1). For phosphates and sulfates, a similar trend is seen, as monophosphate (z = -2) did not phase separate with R_{10}, whereas pyrophosphate (z = -3) did. AMP and NADH were an exception and formed coacervates with R_{10} even though both molecules only have two negative charges. This can be explained by the cation-π interactions of R_{10} with the nucleotide bases, which strengthen the overall intermolecular interactions between the metabolite and R_{10}, and is in agreement with previous

10.1002/syst.202200004

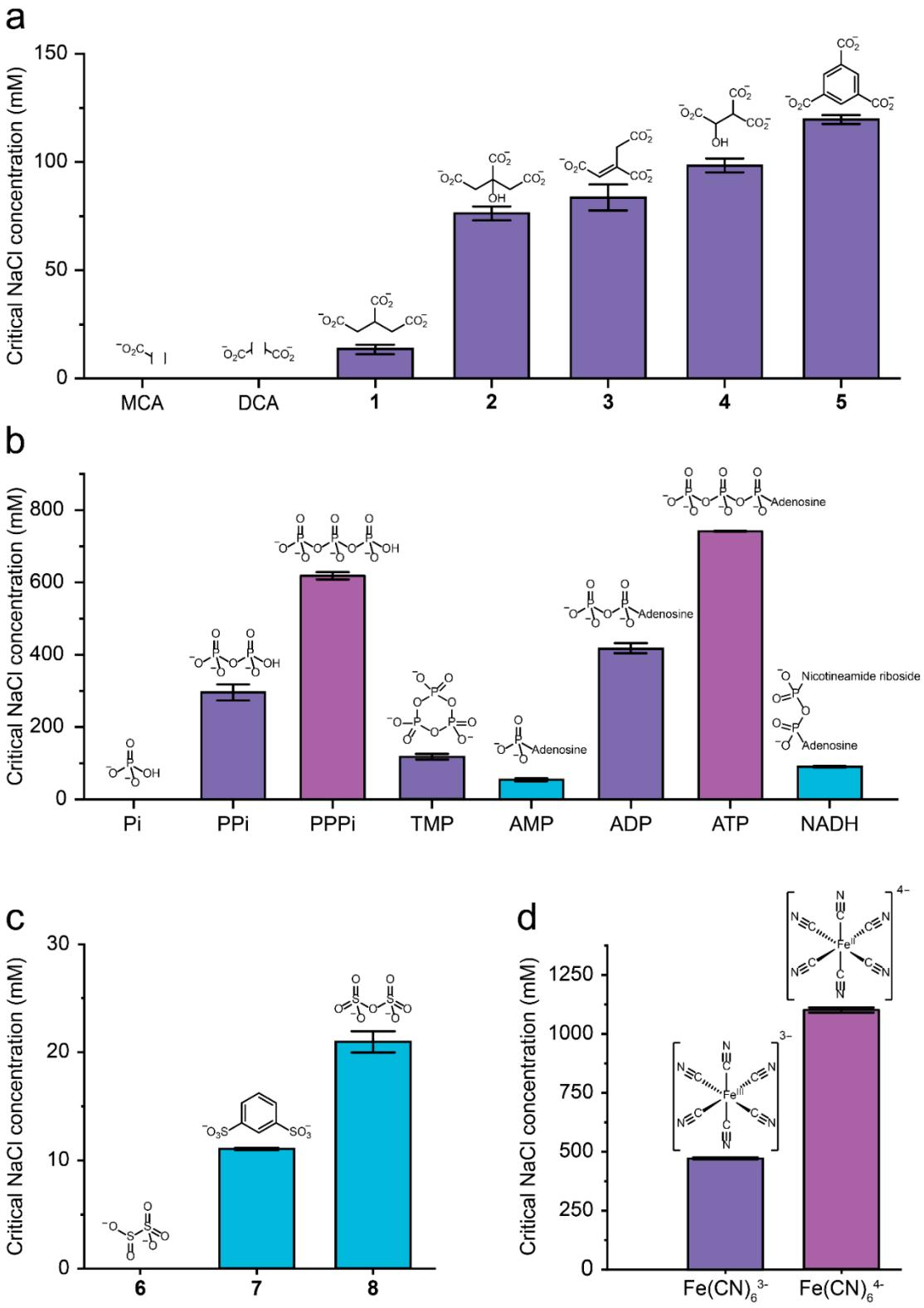

Figure 1. Critical salt concentrations of coacervate forming metabolites with oligoarginine. (a) Tricarboxylic acids phase separate with R_{10} while monocarboxylic acid (MCA) and dicarboxylic acid (DCA) do not. (b) Phosphates containing two negative charges (blue) accompanied by a nucleobase can form coacervates with R_{10}. (c) Sulfates with two negative charges form coacervates with R_{10} while sulfites do not. (d) Ferri- and ferrocyanide coacervates have relatively high critical salt concentrations while not containing aromatic groups. Critical salt concentrations were determined by turbidity measurements and error bars represent the standard deviation (n = 3). Empty regions between brackets indicate a variety of groups (Table S1). Concentration of all molecules is 5 mM (monomer units for R_{10}) or 10 mM for sulfites and sulfates.

observations[24]. Interestingly, pyrosulfate (**8**) was also able to phase separate with R_{10}, while having only two negative charges and no additional interacting groups. We attribute this to the high charge density and number of π electrons, which enhance pyrosulfate's ability to phase separate. Bisulfite did not phase separate with R_{10}, which supports the hypothesis that the π-electrons in the oxygen sp^2 bond interacts with R_{10} and contribute to phase separation.

To quantify the tendency of small metabolites to phase separate with cationic peptides, such as R_{10}, we determined the critical salt concentration (CSC) for each coacervate by titrating the coacervate suspension with NaCl (Figure 1, Table S1). Differences in stability between different coacervates can be caused by the number and strength of interaction sites of their components.[20] For example, the guanidinium groups of R_{10} form relatively strong charge-charge interactions with carboxylate groups compared to the cation-π interactions they form with aromatic groups. The number of charged interaction sites will thus have a large effect on the overall coacervate stability, whereas an increase in cation-π interactions will give a small increase in stability, and the ability to form hydrogen bonds an even smaller increase.[20] For the tricarboxylic acids, which all have three negatively charged groups, a higher CSC was found with an increasing number or strength of additional interaction sites (Figure 1a). For example, the additional hydroxyl group of citrate (**2**) and π bond of trans-aconitate (**3**) increased the CSC by 55 and 65 mM, respectively, compared to coacervates formed by R_{10} and tricarballylate (**1**). Trimesate had the highest CSC of all tricarboxylic acid coacervates, which can be explained by the presence of the benzene ring that forms relatively strong cation-π interactions with R_{10} compared to the other additional interactions.[20]

For phosphate metabolites, a similar trend was observed: the CSC is determined in the first place by the number of negative charges, and secondly by additional interactions such as cation-π interactions (Figure 1b). The CSC of R_{10}/triphosphate (PPPi) coacervates was 300 mM higher than R_{10}/pyrophosphate (PPi) coacervates due to the extra negatively charged phosphate group, whereas the CSC of R_{10}/ATP coacervates was 100 mM higher than that of R_{10}/PPPi coacervates because of the additional adenosine. Moreover, the CSC of R_{10}/NADH coacervates was nearly double that of R_{10}/AMP coacervates, demonstrating a nucleoside group can greatly increase coacervate stability. We also included

trimetaphosphate (TMP), which is a cyclic version of triphosphate and contains three negative charges. Interestingly, R_{10}/TMP coacervates have a significantly lower CSC than R_{10}/PPi coacervates (116.47 mM compared to 296.52 mM, respectively), while both molecules have the same net charge (z = -3) and interacting groups. We attribute this decrease in coacervate stability to the lower flexibility of TMP compared to PPi, which reduces the number of dynamic interactions it can make with R_{10}, an effect that has been observed in coacervates composed of polylysine and DNA.[31] When comparing the general stability of coacervates composed of phosphates compared to carboxylates, it becomes clear that the phosphate coacervates have higher CSCs at similar charge. This can possibly be explained by the higher charge density of the phosphates, as the anionic groups are not separated by an alkyl spacer like in tricarboxylic acids. An additional cause could come from their relative hardness (which manifests itself in a Hofmeister series), leading to a stronger hydration of phosphates.[32] Complex coacervation would release some of the bound water molecules, making phase separation with phosphates more favorable.

In the sulfite and sulfates section, it was found that R_{10}/pyrosulfate (**8**) coacervates had a higher CSC than R_{10}/1,3-benzenedisulfate (**7**) coacervates, which was surprising, as **7** contains an extra benzene group that forms cation-π interactions with R_{10} (Figure 1c). A possible reason for this could be the reduced flexibility of **7** compared to **8**, though it should be noted that a CSC difference of lower than 10 mM could have other causes and a wider range of compounds with varying charge densities should be used to determine the effect of molecular flexibility on electrostatic phase separation.

Lastly, it is striking how high the measured CSC of ferri- and ferrocyanide coacervates was compared other anions with three or four negative charges (Figure 1d). A reason for this could be that ferri- and ferrocyanide structurally contain six negative charges, which are countered by the ferric or ferrous cation to reach a net charge state of -3 and -4, respectively. This means that R_{10} can effectively form more interactions with the iron complexes than with pyrophosphate, for example. Additionally, the π-electrons of the cyanide ligands could contribute to the coacervate stability by interacting with the sp^2 hybridized guanidinium group of arginine, while the lone pairs on the nitrogen can form hydrogen bonds. All these factors make ferri- and ferrocyanide coacervates incredibly stable compared to other small molecule coacervates.

Finally, it should be noted that the CSCs discussed here are determined from R_{10}/metabolite coacervates, and replacing R_{10} with a shorter polycation such as R_5 would decrease the CSC of the coacervates or completely prevent LLPS from occurring.[33] In addition to R_{10}, we also investigated the stability of K_{10}/metabolite coacervates to determine the difference between arginine and lysine in complex coacervation (Table S1). K_{10} was not able to form coacervates with any of the tricarboxylic acids or sulfates used in this study. The CSCs of all K_{10}/phosphate coacervates were significantly lower than R_{10}/phosphate coacervates and TMP, AMP and NADH did not phase separate with K_{10} while they do with R_{10}. These results confirm the consensus that arginine has a higher propensity to phase separate as a result of the stronger cation-π and additional π–π interactions of arginine's guanidinium group compared to the amine group of lysine.[24, 34-35]

Taken together, these results show how small metabolites can form coacervate protocells with a relatively short polycation. It is important to note that we did not investigate the long-term stability of these coacervates against Ostwald ripening[36-37] or coalescence,[38-39] both of which are important for their application potential as protocell models. We generally observed rapid coalescence in our coacervate samples, typical for pure viscous liquid droplets. To stabilize such protocells, strategies involving membranes[38, 40] or active formation may be explored.[37, 41-42]

Active formation of coacervates by aldol addition

We then asked if compartmentalization of these metabolites is compatible with their conversion by metabolic reactions, which is a prerequisite for a primitive metabolism in coacervate protocells. We expect that metabolism and coacervate compartments are mutually dependent: metabolic reactions could affect the coacervates by inducing phase separation or affecting their stability, but coacervates can also affect the rates of metabolism, analogous to the interplay between cellular processes and membraneless organelles.[43-44] Here, we show that conversion of metabolites can induce phase separation, that the conversion of metabolites can be enhanced inside coacervates, and that metabolic reactions taking place inside coacervates can affect their stability and ultimately lead to their dissolution.

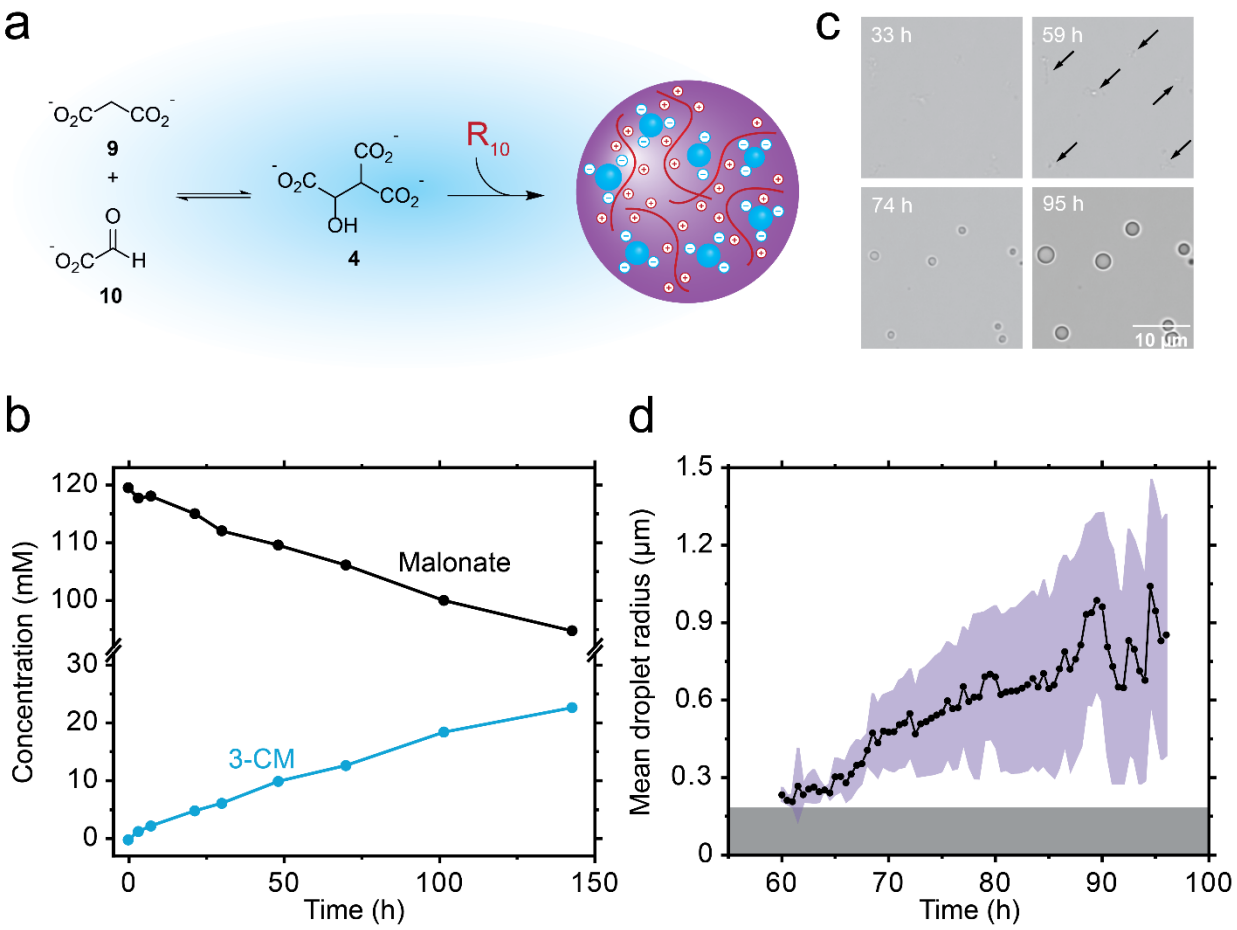

Figure 2 Active formation of coacervates. (a) Aldol addition reaction between dianion malonate (**9**) and glyoxylate (**10**) generates 3-carboxymalate (3-CM, **4**). The trianionic product can undergo LLPS with R_{10}. (b) Plot of concentrations over time for the reaction of 120 mM monosodium malonate with 120 mM sodium glyoxylate in the presence of 5 mM R_{10} as observed by ^{1}H-NMR spectroscopy with 10 mM 3-(trimethylsilyl)propionic-2,2,3,3-d_4 acid sodium salt internal standard. (c) Brightfield microscopy images for the reaction of 120 mM monosodium malonate with 120 mM sodium glyoxylate in the presence of 5 mM R_{10}, showing the formation of coacervates as the reaction progresses. (d) Analysis of droplet size over time. Droplet area was converted to radius and mean droplet radius was calculated. Shaded areas indicate the standard deviation over all droplets in the frame (purple) and detection limit resulting from the threshold in droplet size analysis script (grey).

Metabolic reactions of the compounds shown in Figure 1 can drive phase separation if the product of the reaction has stronger interactions with another species, such as R_{10}. Previous work has shown that the enzymatic conversion of ADP to ATP, which involves the introduction of an additional negative charge, can induce phase separation.[37, 45] Although the use of enzymes is far from prebiotically relevant, reactions involving the addition or removal of charged groups are ubiquitous in prebiotic pathways as well. Several reactions in the tricarboxylic acid (TCA) cycle and its prebiotic analogues introduce additional carboxylate groups.[4-5] To determine whether such prebiotic reactions could give rise to active coacervate formation, we investigated the aldol addition reaction of 120 mM of the diacid malonate (**9**) with 120 mM glyoxylate

(**10**) to form the triacid 3-carboxymalate (3-CM, **4**), shown schematically in Figure 2a.[5] 3-CM should be able to undergo LLPS with 5 mM R_{10}, according to our results in Figure 1. Analysis by ^{1}H-NMR spectroscopy (Figure 2b, SI Figure S1) shows formation of 3-CM after 143 hours in a 22.8% yield. Similar yields were obtained in absence of R_{10} (SI Figure S2-3). Nucleation of coacervate droplets could be seen after 59 hours under the microscope at a concentration of 11 mM 3-CM, after which the coacervate droplets continued to grow (Figure 2c, Supplementary Movie 1). Figure 2d shows the increase in average droplet size over time, which resembles previous observations of actively growing coacervate droplets.[37] A similar result was obtained for the aldol addition reaction between α-ketoglutarate and glyoxylate, which forms the tricarboxylic acids isocitroyl formate and aconitoyl formate (SI Figure S4-7). These results show that metabolite-containing coacervate protocells can be formed through prebiotically relevant metabolic conversions.

Oxidation of NADH is enhanced inside coacervates

After the observation of coacervate formation by conversion of malonate to 3-CM, we investigated if the newly formed protocells could facilitate reactions involving metabolites. Recently, it was shown that simple coacervates can increase the rate of an aldol reaction,[22] which inspired us to investigate the influence of coacervates on a simple redox reaction. NADH was selected as reducing agent because of its prebiotically plausible synthesis and importance in metabolic networks,[46-47] and the possibility to monitor it by fluorescence microscopy and UV spectroscopy. NADH was sequestered in the R_{10}/3-CM coacervates formed in the previous section with a partitioning coefficient (K_p) of 91 ± 4.6, meaning that the NADH concentration inside the coacervate droplets is nearly two orders of magnitude higher than in the dilute phase (Figure 3a). We hypothesized that the locally increased concentrations inside coacervates can increase the rate of NADH-mediated reduction reactions (Figure 3b). We studied the conversion of NADH to NAD^+ by ferricyanide, an anionic oxidizing agent with a partitioning coefficient of 49.6 ± 5.2 in R_{10}/3-CM coacervates and a possible presence on prebiotic Earth.[29] The oxidation of NADH was followed by measuring the absorbance at 340 nm (SI Figure S8), for 30 minutes after the addition of a stoichiometric amount of ferricyanide. A sample containing L-arginine instead of R_{10} was used as a reference without coacervates.

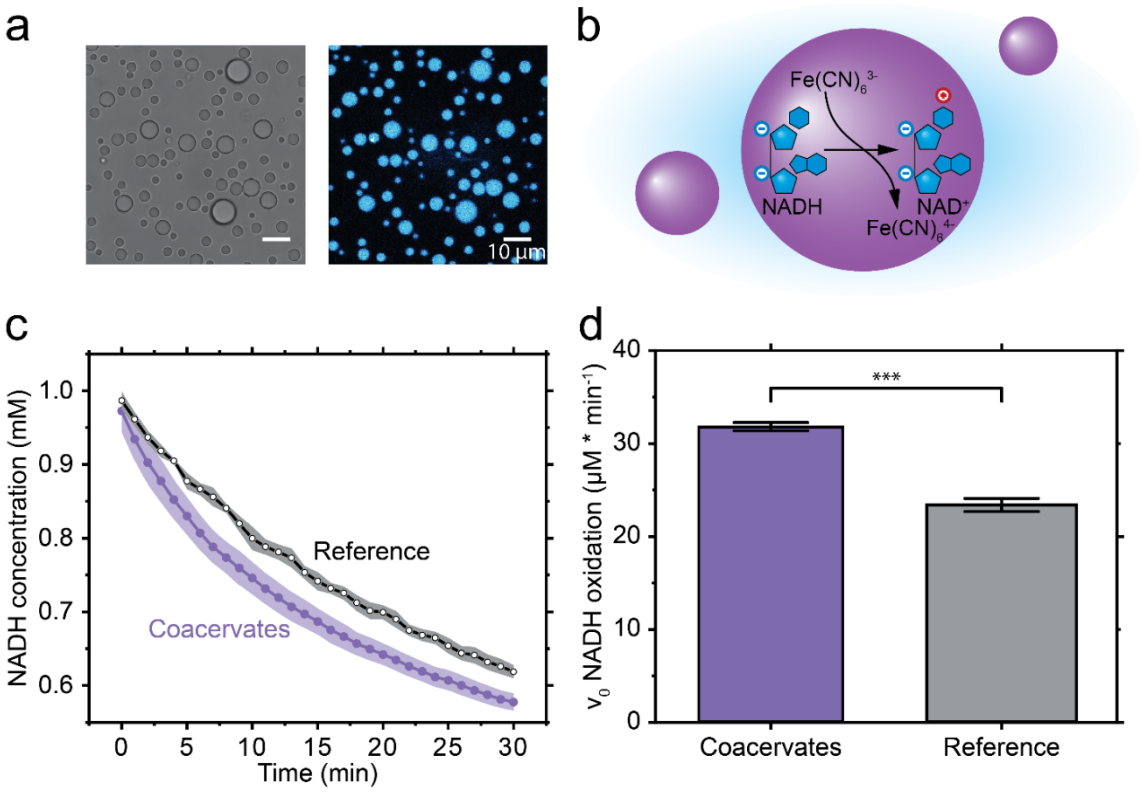

Figure 3. Oxidation of NADH is enhanced by coacervate droplets. (a) Microscopy pictures of R_{10}/3-CM coacervates containing 1 mM NADH in brightfield (left) and excited with a 405 nm laser (right). (b) NADH oxidation by ferricyanide inside coacervate droplets. (c) Oxidation of NADH by $Fe(CN)_6^{3-}$ is increased in the presence of R_{10}/3-CM coacervates (purple, filled) compared to the reference reaction containing Arg/3-CM (black, open). (d) The initial rate (v_0) at which NADH is oxidized is increased in coacervate droplets. Absorbance was measured at 340 nm and a background measurement containing 1mM NAD^+ and 2 mM ferrocyanide in R_{10}/3-CM coacervates or Arg/3-CM solution was subtracted from the measured data. Shaded regions and error bars represent the standard deviation (n = 3). v_0's are significantly different (***) in a two-sample t-test ($p < 0.001$).

We observed a significantly and consistently faster decrease in absorbance at 340 nm for the reaction containing R_{10}/3-CM coacervates compared to the reference reaction, indicating that NADH oxidation by ferricyanide is enhanced by their accumulation in coacervate droplets. The initial reaction rate (v_0) was determined from a linear fit to the first three minutes of the reaction after addition of ferricyanide (SI Figure S9). The initial rate of oxidation of compartmentalized NADH was 1.4 times higher than that of NADH in the reference reaction, 31.8 and 23.4 µM * min^{-1}, respectively. The fact that coacervates can increase the rate of redox reactions has been shown before, but has thus far been limited to enzyme driven systems.[48] To verify that the v_0 increase is due to compartmentalization of NADH and not a difference in pH between the coacervates and surrounding solution, the pH was measured over the course of the reaction. For both conditions, the pH slightly dropped during the reaction, but the difference

between the phase separated and reference reaction was never greater than 0.1 (SI Figure S10). These results show that coacervates can sustain and increase NADH oxidation, a process crucial for electron transport in biology. This is important, as chemical activity would have been essential for protocells and raises the possibility that similar coacervates composed of other metabolites shown in Figure 1 or mixtures of metabolites could have acted as microreactors in a prebiotic environment.

Oxidative decarboxylation of α-keto acids affects stability of coacervate protocells

Finally, having found that coacervates can affect the rate of oxidation of NADH, we wondered whether, vice versa, protometabolic reactions could also affect the coacervate protocells. To this end, we investigated the oxidative decarboxylation of the α-keto acids isocitroyl formate (**11**) and aconitoyl formate (**12**) to form isocitrate (**13**) and aconitate (**3**), by reacting with hydrogen peroxide (Figure 4a). This reaction leads to loss of a keto group (C=O), producing anions that are likely to form less stable coacervates with R_{10} than their precursors (cf. Figure 1). In addition, the carboxylic acid products have a higher pK_a than the α-keto acid substrates and have a slightly lower net charge. And lastly, the oxidative decarboxylation produces CO_2, which can dissolve in the aqueous solution and dissociate into bicarbonate and a proton, thereby lowering the pH and increasing the ionic strength of the solution. Since the stability and physicochemical properties of complex coacervates are highly dependent on ionic strength and pH of the solution, such a reaction could significantly affect the nature of the coacervate protocells.[43, 49-50]

We started by investigating the reaction of 15.2 mM isocitroyl formate and 4.1 mM aconitoyl formate with 5.9 equivalents hydrogen peroxide in Milli-Q water by ^{1}H-NMR spectroscopy (Figure 4b), and observed that the oxidation reaction is completed in less than one hour, having a similar rate in absence or presence of R_{10} (SI Figure S12). As the reaction progressed, a significant decrease in pH was measured, starting at 8.42 before the reaction, and decreasing to 6.10 at the end of the reaction (SI Table S2). Control experiments in which an equal amount of hydrogen peroxide was added to Milli-Q water only showed a decrease in pH from 6.28 to 5.66 (SI Table S3), indicating that the addition of hydrogen peroxide alone is not the reason for the significant lowering of pH. Instead, the CO_2 produced during

decarboxylation of isocitroyl formate and aconitoyl formate partly dissolves and dissociates into bicabonate, which causes the decrease in pH.

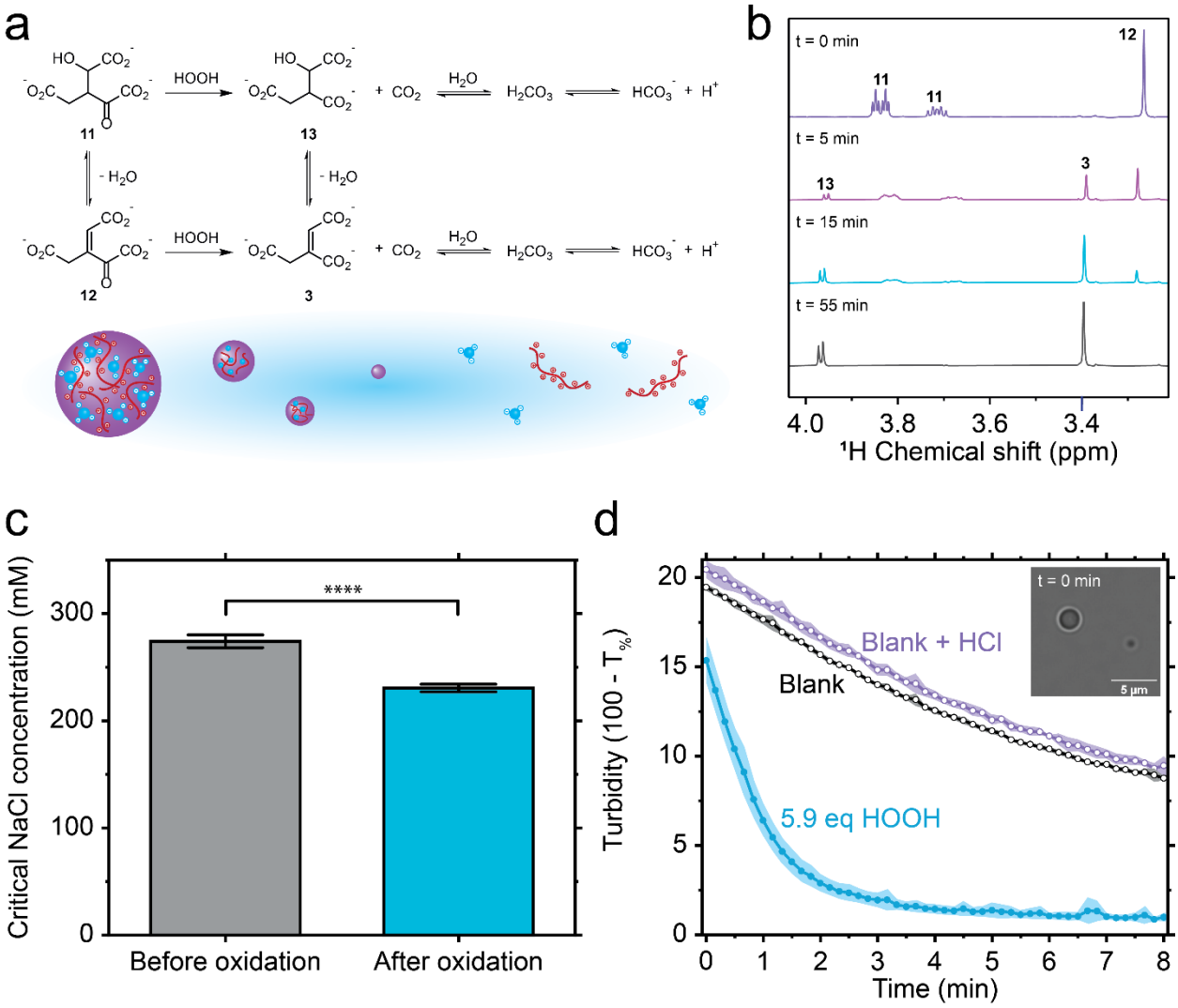

Figure 4: Oxidative decarboxylation of isocitroyl formate and aconitoyl formate decreases coacervate stability. (a) Isocitroyl formate (**11**) and aconitoyl formate (**12**) undergo oxidative decarboxylation by hydrogen peroxide (HOOH) to form isocitrate (**13**) and aconitate (**3**), respectively. During the reaction, carbon dioxide is formed, which dissolves in water and decreases the pH due to dissociation into bicarbonate and a proton. (b) Detail of ^{1}H-NMR spectra over time of the reaction of 15.2 mM isocitroyl formate and 4.1 mM aconitoyl formate with 5.9 equivalents hydrogen peroxide and 1.05 mM 3-(trimethylsilyl)propionic-2,2,3,3-d$_4$ acid sodium salt internal standard, showing the disappearance of **11** and **12** and the formation of **13** and **3**. The full ^{1}H-NMR spectra can be found in SI Figure S11. (c) Decrease in critical salt concentration of coacervates made with 15.2 mM isocitroyl formate, 4.1 mM aconitoyl formate and 5 mM R_{10} upon oxidation by 5.9 eq hydrogen peroxide. Error bars represent the standard deviation. Critical salt concentrations are significantly different (****) in a two-sample *t*-test ($P < 0.0001$). (d) Decrease in turbidity over time upon addition of 3.5 µL 10 wt% (5.9 eq) hydrogen peroxide to coacervates made of 15.2 mM isocitroyl formate, 4.1 mM aconitoyl formate and 5 mM R_{10} in the presence of 235 mM sodium chloride. Blanks where the same volume of Milli-Q water and 0.4 mM hydrochloric acid (resulting in a similar decrease in pH as for addition of hydrogen peroxide to water) were added as reference. The standard deviation is depicted as shading around the curves. Insert: Coacervate droplets as observed by Brightfield microscopy.

We then investigated what the effect of the reaction is on the stability of the coacervate protocells. We measured the critical salt concentration of coacervates made of 15.2 mM isocitroyl formate and 4.1 mM aconitoyl formate with 5 mM R_{10}, before and after the reaction with 5.9 equivalents hydrogen peroxide (Figure 4c), and observed a significant decrease in CSC from 274.1 ± 3.2 mM to 230.5 ± 2.0 mM due to the oxidative decarboxylation reaction. Control experiments performed in 100 mM MOPS buffer (pH 7.55) showed a difference in CSC of 11.8 mM (SI Figure S13), indicating that decreased coacervate stability can be explained by a combination of decreased interaction strength of the reaction products, isocitrate / aconitate with R_{10}, and the concomitant decrease in pH and increase in ionic strength due to bicarbonate formation. Such a decrease in CSC and change in composition of the coacervates is expected to coincide with a change in physicochemical properties of the protocell, including viscosity and surface tension.[51-53] Moreover, at specific conditions, this protometabolic reaction could be used to dissolve the compartments in which the reaction is taking place. To test this, we again prepared coacervate samples made of 15.2 mM isocitroyl formate and 4.1 mM aconitoyl formate with 5 mM R_{10}, but now added 235 mM NaCl. This value was chosen to be in between de CSCs of the reagents and products, so that reaction with 5.9 eq hydrogen peroxide would result in dissolution of the coacervates. We followed the turbidity of the reaction over time by plate reader, and indeed observed a disappearance of turbidity after 5 minutes (Figure 4d), indicating that the coacervates had fully dissolved. Control experiments where an equivalent amount of Milli-Q water or 0.4 mM HCl (resulting, in pure water, in a similar pH drop as the hydrogen peroxide) was added, only showed a gradual decrease in turbidity due to settling of the coacervate droplets. This shows that metabolic reactions, such as the oxidative decarboxylation of isocitroyl formate and aconitoyl formate, can have a significant effect on the stability of the coacervate protocells, and can even drive their dissolution.

Conclusions

We have shown that coacervate protocells can form by phase separation of a wide range of prebiotically relevant anionic metabolites with R_{10}. The difference in electrostatic stability of the metabolite coacervates made with different anions can be explained by the number of interaction sites, such as charged or aromatic

groups, and the type of anion. This difference in stability can be exploited to actively form coacervates, for example through the conversion of malonate and glyoxylate to 3-carboxymalate. During this reaction, we observed nucleation and steady growth of coacervate droplets. These metabolite coacervates were able to sustain, and even enhance reactions that were localized to the coacervate interior, such as the oxidation of NADH. We found an increase in oxidation rate by 40%, which we attribute to the high local concentration of NADH and ferricyanide inside the coacervates. Lastly, we have shown that protometabolic reactions can also change physicochemical properties of coacervate protocells, and even decrease their stability such that they dissolve. We used the oxidative decarboxylation of isocitroyl formate and aconitoyl formate by hydrogen peroxide to illustrate this effect, and show that the combination of decreased interaction strength of the reaction products and the decrease in pH due to carbonation of the solution leads to a sufficient lowering of the stability to dissolve the coacervate droplets.

The fact that stable coacervate droplets can be formed from a short polycation and small metabolites with as few as two negative charges is significant, as it offers new insights for the development of protocells with more prebiotically plausible materials. Importantly, the coacervates can be made chemically active with protometabolic reactions that produce or consume droplet material, which opens up possibilities to use the latest insights in prebiotic chemistry to generate liquid compartments and to link together compartmentalization and metabolism, two central elements of living systems. A scenario in which coacervate protocells nucleate, grow and eventually dissolve with progression of a reaction cycle would be the next step of protocell construction.

Conflicts of interest

There are no conflicts of interest to declare.

Acknowledgements

The authors would like to thank Annemiek Slootbeek and Dr. Oliver Maguire for useful input and discussions. This project has received funding from the European Research Council (ERC) under the

European Union's Horizon 2020 research and innovation programme under grant agreement number 851963. Tiemei Lu acknowledges the China Scholarship Council (CSC) for support.

References

[1] N. A. Yewdall, A. F. Mason, J. C. M. Van Hest, *Interface Focus* **2018**, *8*, 20180023.
[2] K. Ruiz-Mirazo, C. Briones, A. de la Escosura, *Chem. Rev.* **2014**, *114*, 285-366.
[3] M. Gull, *Challenges* **2014**, *5*, 193-212.
[4] G. Springsteen, J. R. Yerabolu, J. Nelson, C. J. Rhea, R. Krishnamurthy, *Nat. Commun.* **2018**, *9*, 91.
[5] R. T. Stubbs, M. Yadav, R. Krishnamurthy, G. Springsteen, *Nat. Chem.* **2020**, *12*, 1016-1022.
[6] X. V. Zhang, S. T. Martin, *J. Am. Chem. Soc.* **2006**, *128*, 16032-16033.
[7] K. B. Muchowska, S. J. Varma, E. Chevallot-Beroux, L. Lethuillier-Karl, G. Li, J. Moran, *Nat. Ecol. Evol.* **2017**, *1*, 1716-1721.
[8] K. B. Muchowska, S. J. Varma, J. Moran, *Nature* **2019**, *569*, 104-107.
[9] S. Basak, S. Nader, S. S. Mansy, *JACS Au* **2021**, *1*, 371-374.
[10] J. P. Schrum, T. F. Zhu, J. W. Szostak, *Cold Spring Harb Perspect. Biol.* **2010**, *2*, a002212.
[11] S. Koga, D. S. Williams, A. W. Perriman, S. Mann, *Nat. Chem.* **2011**, *3*, 720-724.
[12] R. Krishnamurthy, *Acc. Chem. Res.* **2017**, *50*, 455-459.
[13] Y. A. Takagi, D. H. Nguyen, T. B. Wexler, A. D. Goldman, *J. Mol. Evol.* **2020**, *88*, 598-617.
[14] I. A. Chen, P. Walde, *Cold Spring Harb. Perspect. Biol.* **2010**, *2*.
[15] P. A. Monnard, P. Walde, *Life* **2015**, *5*, 1239-1263.
[16] T. A. Hyman, C. P. Brangwynne, *Nature* **2012**, *491*, 524-525.
[17] M. H. I. van Haren, K. K. Nakashima, E. Spruijt, *J. Syst. Chem.* **2020**, *8*, 107-120.
[18] M. Abbas, W. P. Lipiński, J. Wang, E. Spruijt, *Chem. Soc. Rev.* **2021**, *50*, 3690-3705.
[19] H. G. Bungenberg de Jong, H. R. Kruyt, *Proc. K. Ned. Akad. Wet.* **1929**, 849-856.
[20] C. P. Brangwynne, P. Tompa, R. V. Pappu, *Nat. Phys.* **2015**, *11*, 899-904.
[21] R. R. Poudyal, R. M. Guth-Metzler, A. J. Veenis, E. A. Frankel, C. D. Keating, P. C. Bevilacqua, *Nat. Commun.* **2019**, *10*.
[22] M. Abbas, W. P. Lipiński, K. K. Nakashima, W. T. S. Huck, E. Spruijt, *Nat. Chem.* **2021**, 1046-1054.
[23] L. Zhou, J. J. Koh, J. Wu, X. Fan, H. Chen, X. Hou, L. Jiang, X. Lu, Z. Li, C. He, *Bioconjugate Chem.* **2022**.
[24] F. P. Cakmak, S. Choi, M. O. Meyer, P. C. Bevilacqua, C. D. Keating, *Nat. Commun.* **2020**, *11*, 5949.
[25] H. Kim, B. J. Jeon, S. Kim, Y. Jho, D. S. Hwang, *Polymers* **2019**, *11*.
[26] S. Lenton, S. Hervø-Hansen, A. M. Popov, M. D. Tully, M. Lund, M. Skepö, *Biomacromolecules* **2021**, *22*, 1532-1544.
[27] J. W. Bye, R. A. Curtis, *J. Phys. Chem. B* **2019**, *123*, 593-605.
[28] M. A. Keller, D. Kampjut, S. A. Harrison, M. Ralser, *Nat. Ecol. Evol.* **2017**, *1*, 83.
[29] A. D. Keefe, S. L. Miller, *Origins Life Evol. Biospheres* **1996**, *26*, 111-129.
[30] R. Liu, L. E. Orgel, *Origins Life Evol. Biospheres* **1998**, *28*, 245-257.
[31] A. Shakya, J. T. King, *Biophys. J.* **2018**, *115*, 1840-1847.
[32] P. Mohammadi, C. Jonkergouw, G. Beaune, P. Engelhardt, A. Kamada, J. V. I. Timonen, T. P. J. Knowles, M. Penttila, M. B. Linder, *J. Colloid Interface Sci.* **2020**, *560*, 149-160.
[33] E. Spruijt, A. H. Westphal, J. W. Borst, M. A. Cohen Stuart, J. van der Gucht, *Macromolecules* **2010**, *43*, 6476-6484.
[34] I. Alshareedah, T. Kaur, J. Ngo, H. Seppala, L. D. Kounatse, W. Wang, M. M. Moosa, P. R. Banerjee, *J. Am. Chem. Soc.* **2019**, *141*, 14593-14602.
[35] T. Lu, K. K. Nakashima, E. Spruijt, *J. Phys. Chem. B* **2021**, *125*, 3080-3091.
[36] M. Tena-Solsona, J. Janssen, C. Wanzke, F. Schnitter, H. Park, B. Rieß, J. M. Gibbs, C. A. Weber, J. Boekhoven, *ChemSystemsChem* **2021**, *3*, e2000034.

[37] K. K. Nakashima, M. H. I. van Haren, A. A. M. André, I. Robu, E. Spruijt, *Nat. Commun.* **2021**, *12*, 3819.
[38] M. Matsuo, K. Kurihara, *Nat. Commun.* **2021**, *12*, 5487.
[39] J. Berry, S. C. Weber, N. Vaidya, M. Haataja, C. P. Brangwynne, *Proc. Natl. Acad. Sci. U. S. A.* **2015**, *112*, E5237-5245.
[40] A. F. Mason, B. C. Buddingh, D. S. Williams, J. C. M. van Hest, *J. Am. Chem. Soc.* **2017**, *139*, 17309-17312.
[41] D. Zwicker, A. A. Hyman, F. Jülicher, *Phys. Rev. E: Stat., Nonlinear, Soft Matter Phys.* **2015**, *92*, 012317.
[42] C. Donau, F. Späth, M. Sosson, B. A. K. Kriebisch, F. Schnitter, M. Tena-Solsona, H. S. Kang, E. Salibi, M. Sattler, H. Mutschler, J. Boekhoven, *Nat. Commun.* **2020**, *11*, 5167.
[43] K. K. Nakashima, M. A. Vibhute, E. Spruijt, *Front. Mol. Biosci.* **2019**, *6*, 21.
[44] W. Peeples, M. K. Rosen, *Nat. Chem. Biol.* **2021**, *17*, 693-702.
[45] K. K. Nakashima, J. F. Baaij, E. Spruijt, *Soft Matter* **2018**, *14*, 361-367.
[46] M. J. Dowler, W. D. Fuller, L. E. Orgel, R. A. Sanchez, *Science* **1970**, *169*, 1320-1321.
[47] C. Bonfio, E. Godino, M. Corsini, F. F. de Biani, G. Guella, S. S. Mansy, *Nat. Catal.* **2018**, *1*, 616-623.
[48] T. Ura, S. Tomita, K. Shiraki, *Chem. Commun. (Cambridge, U. K.)* **2021**, *57*, 12544-12547.
[49] J. van der Gucht, E. Spruijt, M. Lemmers, M. A. Cohen Stuart, *J. Colloid Interface Sci.* **2011**, *361*, 407-422.
[50] S. L. Perry, *Curr. Opin. Colloid Interface Sci.* **2019**, *39*, 86-97.
[51] J. Qin, D. Priftis, R. Farina, S. L. Perry, L. Leon, J. Whitmer, K. Hoffmann, M. Tirrell, J. J. De Pablo, *ACS Macro Lett.* **2014**, *3*, 565-568.
[52] Y. Liu, B. Momani, H. H. Winter, S. L. Perry, *Soft Matter* **2017**, *13*, 7332-7340.
[53] E. Spruijt, J. Sprakel, M. A. C. Stuart, J. van der Gucht, *Soft Matter* **2010**, *6*, 172-178.

Footnotes

‡ These authors contributed equally.